PWM DUAL INVERTER BASED GRID CONNECTED PV SYSTEM WITH SLIDING MODE CONTROL

SANDARI VENKATA VIJAYA GANESH[1]
[1]Student, dept. of Electrical and Electronics Engineering, JNTUA Anantapuram.

ABSTRACT: ***This paper presents a novel robust & adaptive sliding mode (SM) control for a cascaded two-level inverter (CTLI)-based grid connected photovoltaic (PV) system. The modelling and design of the control scheme for the CTLI-based grid connected PV system is developed to supply active power and reactive power with variable solar irradiance. There are two different switching schemes have been used to design the SM controllers. The performance of the SM controller is improved by using an adaptive hysteresis-band (HB) calculation. To improve the performance of SMC further, the present work develops a fuzzy controller for a nonlinear system allows for a reduction of uncertain effects in the system control and improve the efficiency. The controller performance is found to be satisfactory for both the schemes at considered load and solar irradiance level variations in simulation environment. The proposed controller is found to be capable of implementing the control algorithm successfully in the considered situation.***

Index Terms: Photovoltaic (PV) system, multilevel inverter, Fuzzy controller, Vector control, sliding mode control (S M C) .

I.INTRODUCTION

Photovoltaic (PV) energy is accepted as a popular source of non-conventional energy due to a number of benefits, particularly low operational cost and less pollution. Throughout the world, photovoltaic power generation is becoming increasingly popular due to a combination of factors: low maintenance, minimal wear and tear of components due to the absence of moving parts, lack of audible noise, absence of fuel cost, and pollution-free operation after installation. Small-scale PV installations are very popular as lighting and water pumping solutions in developing countries, remote villages, and small rural and urban communities. These systems are also commonly used in developed countries that have a considerable amount of solar irradiation.

The multilevel voltage source converters have emerged as one of the preferred choices for medium voltage (MV) high-power applications due to several advantages. Some of the most popular topologies of multilevel voltage- source converters are neutral point or diode-clamped converters (NPC), flying-capacitor (FC) converters and cascaded H-Bridge converters (CHB). SMC is one of the effective nonlinear robust control approaches since it provides system dynamics with an invariance property to uncertainties once the system dynamics are controlled in the sliding mode. Some PV systems, using power conversion for grid interfacing have been proposed. The cascaded H-bridge converter receives large attention among these topologies, due to the modular circuit layout. The major advantage of CHB over other topologies is a minimal requirement of dc sources; the number of levels in the output voltage can be increased. One of the robust and dynamic control techniques is the sliding mode control (SMC). The control of the capacitor voltage is developed using a vector control scheme. In this work, the PV modules are designed to produce a dc voltage of 48 V under rated Indian solar irradiance. The photovoltaic systems are connected to the CTLI, and inverter output to the low voltage (LV) side of an open winding three-phase transformer. The complete power scheme is shown in Fig.1

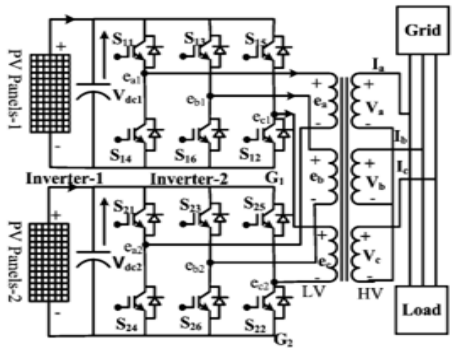

Fig.1 Power circuit of the photovoltaic system with cascaded two level inverter

The paper discusses the problem with following Contributions:

i) Two isolated PV sources are designed to supply active power at 48 V at a normal Indian solar irradiance. This ensures the maximum power delivery of the system at rated condition.

ii) A novel SM control scheme is proposed so that the CTLI based system and also in the absence of solar irradiance.

iii) The controllers are designed for two different switching schemes,

(A) Two-Level Switching and

(B) Forced Switching.

iv) The input solar irradiance is varied and also reduced to zero to establish the operation of the control with variable level of active power supply and reactive power supply.

v) The modulation technique for the CTLI is established with a simple PWM technique instead of referring Space Vector modulation technique.

II.MATHEMATICAL MODELLING OF THE SYSTEM NOMENCLATURE:

V = Solar cell terminal voltage [V]
I = Solar cell terminal current [A]
$I_{ph.}$ = Photo generated current [linear with irradiance]
I_S = Saturation current due to diffusion mechanism
T = Cell temperature [K]
K = Boltzmann's constant
q = Electron charge
n = Diode quality factor [silicon diode n =2]
R_S =Cell series resistance [Ω]
R_{sh} = Cell shunt resistance [Ω]
N_p = Number of parallel cells
N_S = Number of series cells
V_{dc} = dc-link voltage of the voltage source inverter (VSI)
Va, Vb, VC = Per phase grid voltages
ea1, eb1, ec1= First inverter pole voltages
ea2, eb2, ec2 = Second inverter pole voltages
Vq = q-component of the source voltage
Vd = d-component of the source voltage
The characteristic equation of PV cells is given by

$$I = I_{ph} - I_s \left[e^{\frac{q(V+IRs)}{nKT}} - 1\right] - \frac{V+RsI}{Rsh} \quad (1)$$

The equivalent circuit determined from the equation is used for the simulation model, is shown in Fig. 2. The complete multidimensional array model equation is shown in (2).

$$I = N_p\left[I_{ph} - I_s\left[exp^{\frac{q\left[\left(\frac{V}{N_S}\right)+\left(\frac{I}{N_p}\right)R_S\right]}{KT}} - 1\right] - \frac{\left(\frac{V}{N_S}\right)+\left(\frac{I}{N_p}\right)R_S}{R_{sh}}\right] \quad (2)$$

The number of cells connected in series to form one set, and the number of sets connected in parallel to form one array has been considered to provide maximum power at 48 V at the normal Indian solar irradiance. Power rating of the inverter is taken as 2.5 KW. The available output power at different output voltage is shown in Fig. 3. Here the output power is found to be maximum at 48 V with fixed solar irradiance.

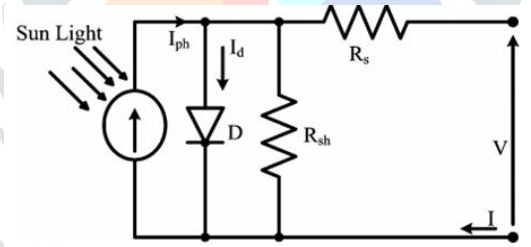

Fig.2. Equivalent circuit of PV cell

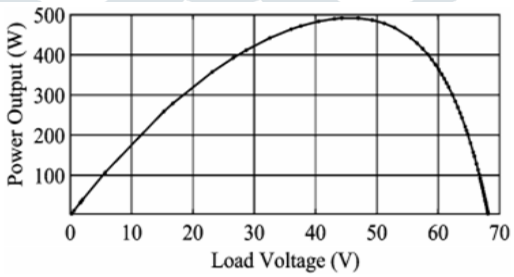

Fig. 3. Power-Voltage characteristics for the PVsystem

Accordingly, the controllers are designed to maintain the total PV output voltage of the two inverters (as shown in Fig. 1) at 96 V, to ensure maximum power delivery by the system.

A. CTLI model

For the considered power scheme, the voltage across a, b and c windings are as follows:

$$e_a = \frac{2}{3}(e_{a1} - e_{a2}) - \frac{1}{3}(e_{b1} - e_{b2}) - \frac{1}{3}(e_{c1} - e_{c2}) \quad (3)$$

$$e_b = -\frac{1}{3}(e_{a1} - e_{a2}) + \frac{2}{3}(e_{b1} - e_{b2}) - \frac{1}{3}(e_{c1} - e_{c2}) \quad (4)$$

$$e_c = -\frac{1}{3}(e_{a1} - e_{a2}) - \frac{1}{3}(e_{b1} - e_{b2}) + \frac{2}{3}(e_{c1} - e_{c2}) \quad (5)$$

Where, are first inverter pole voltages ea1, eb1, ec1 and ea2, eb2, ec2 are second inverter pole voltages. Assuming ideal power switches, the output voltage of the CTLI is obtained as (3), (4) and (5) which can be rewritten in matrix form as (6).

$$\begin{bmatrix} e_a \\ e_b \\ e_c \end{bmatrix} = \frac{1}{3}\begin{bmatrix} 2 & -1 & -1 \\ -1 & 2 & -1 \\ -1 & -1 & 2 \end{bmatrix}\begin{bmatrix} e_{a1} \\ e_{b1} \\ e_{c1} \end{bmatrix} - \frac{1}{3}\begin{bmatrix} 2 & -1 & -1 \\ -1 & 2 & -1 \\ -1 & -1 & 2 \end{bmatrix}\begin{bmatrix} e_{a2} \\ e_{b2} \\ e_{c2} \end{bmatrix} \quad (6)$$

B. Vector control

The two-axis representation of the supply voltages can be formed as:

$$\begin{bmatrix} V_\alpha \\ V_\beta \end{bmatrix} = \frac{1}{3}\begin{bmatrix} 1 & -1/2 & -1/2 \\ 0 & -\sqrt{3}/2 & \sqrt{3}/2 \end{bmatrix}\begin{bmatrix} V_a \\ V_b \\ V_c \end{bmatrix} \quad (7)$$

Accordingly, switching state equations it can be expressed as

$$\begin{bmatrix} V_\alpha \\ V_\beta \end{bmatrix} = \frac{1}{3}\begin{bmatrix} 1 & -1/2 & -1/2 \\ 0 & -\sqrt{3}/2 & \sqrt{3}/2 \end{bmatrix}\begin{bmatrix} V_a \\ V_b \\ V_c \end{bmatrix}\begin{bmatrix} \gamma_{1\alpha} \\ \gamma_{1\gamma} \end{bmatrix} V_{dc1} - \frac{2}{3}\begin{bmatrix} 1 & -1/2 & -1/2 \\ 0 & -\sqrt{3}/2 & \sqrt{3}/2 \end{bmatrix}\begin{bmatrix} \gamma_{2\alpha} \\ \gamma_{2\gamma} \end{bmatrix} V_{dc2} \quad (8)$$

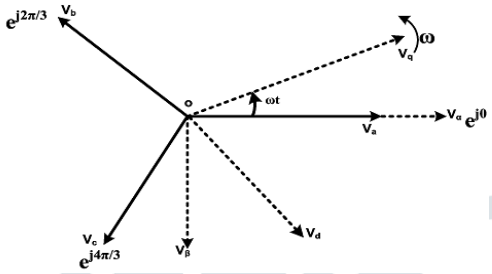

Fig.4. Vector diagram of the voltage

Here, the d-q axis of the used vector control are derived following Fig. 4, and found as:

$$\begin{bmatrix} V_d \\ V_q \end{bmatrix} = \begin{bmatrix} \sin\omega t & \cos\omega t \\ \cos\omega t & -\sin\omega t \end{bmatrix}\begin{bmatrix} V_m \sin\omega t \\ V_m \cos\omega t \end{bmatrix} \quad (9)$$

The equivalent circuit for 'a' phase is shown in Fig. 5, in which Va is the grid voltage, R is the loss representing resistance, L is the leakage inductance of transformer. The transformer is step-up with turn ratio 1: n. Applying KVL for 'a', 'b' and 'c' phases.

$$n\,(e_{a1} - e_{a2}) = R_a\, i_a + L_a\frac{di_a}{dt} + V_a$$

$$n\,(e_{b1} - e_{b2}) = R_b\, i_b + L_b\frac{di_b}{dt} + V_b$$

$$n\,(e_{c1} - e_{c2}) = R_c\, i_c + L_c\frac{di_c}{dt} + V_c \quad (10)$$

R_a, R_b and R_c are considered to be equal to R and the L_a, $L_b$and L_c are equal to L.

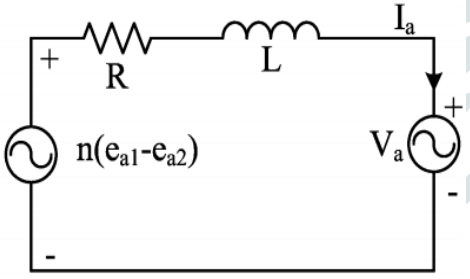

Fig.5. Single phase equivalent circuit

The reference value of d-axis current is generated from dc link voltage controller. In this work, the reference the total of two dc voltage is kept at 96V.

C. Sliding mode control (SMC)

SMC is particularly interesting due to its known characteristics of robustness, system order reduction and appropriateness to the ON–OFF behavior of power switches. The easy implementation of SM control through hysteresis band does not require additional computation or auxiliary circuitries. There are basically three approaches in keeping the switching frequency of the hysteresis modulation (HM)-based SM controller constant.

a) Constant ramp or timing functions directly into the controller. In this control scheme the fixed switching frequency under all operating conditions, and controlled through varying the ramp/timing function.

b) Adaptive control into the HM-based SM controller to counteract the switching frequency variation.

c) Constant switching frequency SM controllers can also be obtained by employing PWM instead of HM.

The cascaded control structure is chosen for ease of control realization and to exploit the motion separation property of power converters. For power converters, the fast motion is dominated by the dynamics of the loop current, whereas the slow motion stems from the dynamics of the output voltage.

Scheme-I: Two-Level Switching

In this scheme, the inverter is operated under bipolar modulation with two levels of output 1 and -1.

Fig. 6 shows the switching logic. For a particular phase of the two inverters, two switches are turned on, and the other two switches are turned off, in each cycle. If f_{sw} is the switching frequency, then the switching loss per on-off is proportional to the switching Frequency and given by PInv = kf sw .The total switching loss is 2 PInv . A variable structure control (u) is described as,

$$u = \begin{cases} +1, if\ S_e > +HB \\ -1, if\ S_e < -HB \end{cases} \quad (11)$$

Where, Se is the error between the actual value of the state variable and its corresponding reference. According to SM theory, Sk crosses the switching surface (Sk) at every switching instant, satisfying the SM conditions. Scheme I, as discussed above, is depicted in Fig. 6.

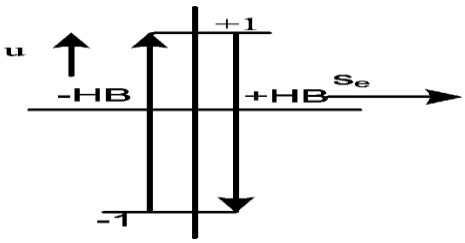

Fig. 6. Two-level hysteresis modulation

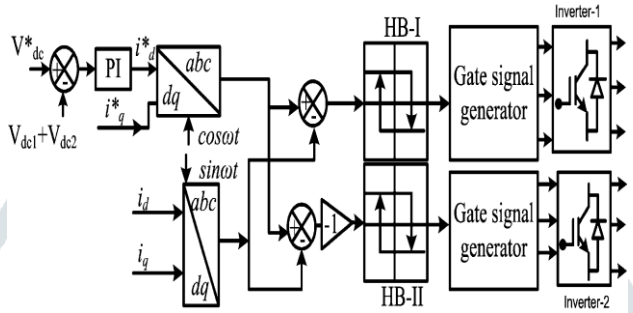

Fig.7.Control block diagram of Scheme-I

Scheme-II : Forced Switching

The carrier signal is triangular in nature. The amplitude of triangular signal is same as the hysteresis band. The technique retains the robustness properties of hysteresis controller while achieving the constant switching frequency. Further, there is a minimum magnitude bound for the carrier signal at different frequencies.

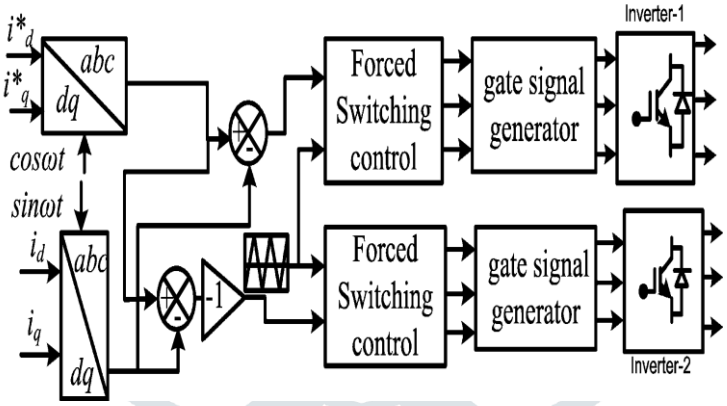

Fig.8.Control block diagram of Scheme-II

To improve the performance of SMC, the present work develops a systematic adaptive procedure to calculate the band of the hysteresis comparators.

Adaptive HB calculation for SMC

The calculation of hysteresis band is accomplished by considering a simple case with purely inductive load. The current reaches the upper and lower hysteresis band following Fig. 9 which, in turn, yields the voltage-current relationship as given by (12) and (13).

$$L\frac{di_a^+}{dt} = V_{dc} \quad (12)$$

$$L\frac{di_a^-}{dt} = -V_{dc} \quad (13)$$

Adding equation

$$L\frac{di_a^+}{dt} + L\frac{di_a^-}{dt} = 0 \quad (14)$$

From the geometry of Fig. 9, it can be found

$$t_1\frac{di_a^+}{dt} - t_1\frac{di_a^*}{dt} = 2HB \quad (15)$$

$$t_2\frac{di_a^-}{dt} - t_2\frac{di_a^*}{dt} = -2HB \quad (16)$$

$$t_1 + t_2 = T_{sw} = \frac{1}{f_{sw}} \quad (17)$$

Where t1 and t2 are the respective switching intervals, and f_{sw} is the modulation frequency.

$$t_1\frac{di_a^+}{dt} + t_2\frac{di_a^-}{dt} - \frac{1}{f_{sw}}\frac{di_a^*}{dt} = 0 \quad (18)$$

Further, subtracting (16) from (15), one obtains

$4HB = t_1 \frac{di_a^+}{dt} - t_2 \frac{di_a^-}{dt} - (t_1 - t_2) \frac{di_a^*}{dt}$ (19)

Now, using (14), (18) and (19) it can be found that

$$4HB = \frac{1}{f_{sw}} \left[\frac{di_a^+}{dt} - \frac{\left(\frac{di_a^*}{dt}\right)^2}{\frac{di_a^+}{dt}} \right] \quad (20)$$

Let $\frac{di_a^*}{dt}$ be denoted by *m*, then (20) can be rewritten as

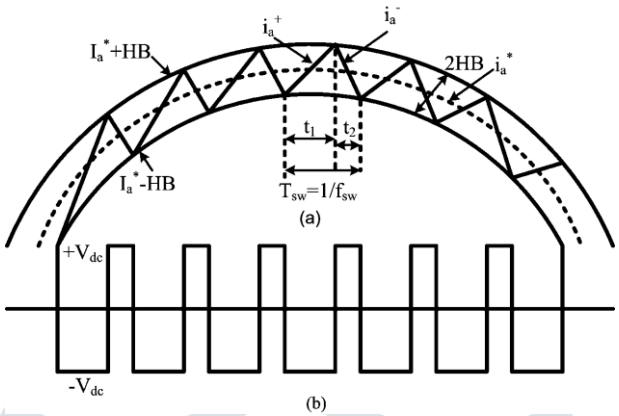

Fig. 9. Time-domain representation of two level hysteresis current controls: (a) current waveforms with hysteresis control, and (b) Voltage source CTLI ac terminal voltage.

$$HB = \frac{0.25V_{dc}}{Lf_{sw}} \left[1 - \frac{(mL)^2}{V_{dc}^2}\right] \quad (21)$$

$$HB = \frac{0.25V_{dc}}{Lf_{sw(max)}} \quad (22)$$

The equation (22) is used to improve the PWM performances of adaptive hysteresis band.

III. SYSTEM CONFIGURATION

The open-end winding of a three-phase transformer low-voltage (LV) side is connected between the two inverters.

The secondary is directly connected to the distribution grid. The transformer parameters are taken as shown in the Table II which is drawing sinusoidal current from the voltage waveform, as shown later in the result section.

TABLE I
TRANSFORMER PARAMETERS

S. No.	PARAMETER	Value
1.	Secondary phase voltage (rms)	400 V
2.	Primary phase voltage (rms)	48 V
3.	Frequency	50 Hz
4.	Power	2.5 KVA
5.	Transformer leakage inductance, L	13 %
6.	Transformer resistance	3 %

IV. FUZZY LOGIC CONTROLLER

In FLC, basic control action is determined by a set of linguistic rules. These rules are determined by the system. Since the numerical variables are converted into linguistic variables, mathematical modeling of the system is not required in FC.

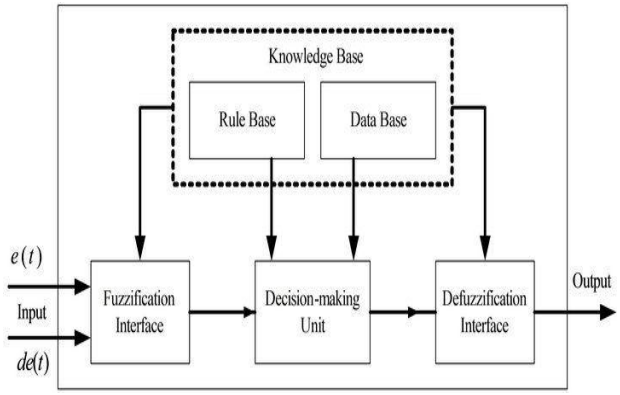

Fig.10.Fuzzy logic controller

The FLC comprises of three parts: fuzzification, interference engine and defuzzification. The FC is characterized as

i. Seven fuzzy sets for each input and output.
ii. Triangular membership functions for simplicity.
iii. Fuzzification using continuous universe of discourse.
iv. Implication using Mamdani's, 'min' operator.
v. Defuzzification using the height method.

TABLE II: Fuzzy Rules

Change in error	Error						
	NB	NM	NS	Z	PS	PM	PB
NB	PB	PB	PB	PM	PM	PS	Z
NM	PB	PB	PM	PM	PS	Z	Z
NS	PB	PM	PS	PS	Z	NM	NB
Z	PB	PM	PS	Z	NS	NM	NB
PS	PM	PS	Z	NS	NM	NB	NB
PM	PS	Z	NS	NM	NM	NB	NB
PB	Z	NS	NM	NM	NB	NB	NB

Fuzzification:

Membership function values are assigned to the linguistic variables, using seven fuzzy subsets: NB (Negative Big), NM (Negative Medium), NS (Negative Small), ZE (Zero), PS (Positive Small), PM (Positive Medium), and PB (Positive Big). The Partition of fuzzy subsets and the shape of membership CE(k). E(k) function adapt the shape up to appropriate system. The value of input error and change in error are normalized by an input scaling factor. In this system the input scaling factor has been designed such that input values are between -1 and +1. The triangular shape of the membership function of this arrangement presumes that for any particular E(k) input there is only one dominant fuzzy subset. The input error for the FLC is given as

$$E(k) = \frac{P_{ph(k)} - P_{ph(k-1)}}{V_{ph(k)} - V_{ph(k-1)}} \quad (23)$$

$$CE(k) = E(k) - E(k\text{-}1) \quad (24)$$

Inference Method:

Several composition methods such as Max–Min and Max-Dot have been proposed in the literature. This proposes a Min method. The output membership function of each rule is given by the minimum operator and maximum operator. Table 1 shows rule base of the FLC.

Defuzzification:

As a plant usually requires a non-fuzzy value of control, a defuzzification stage is needed. To compute the output of the FLC, height method is used and the FLC output modifies the control output. Further, the output of FLC controls the switch in the inverter. In UPQC, the active power, reactive power, terminal voltage of the line and capacitor voltage are required to be maintained. In order to control these parameters, they are sensed and compared with the reference values. To achieve this, the membership functions of FC are: error, change in error and output.

The set of FC rules are derived from

$$u=-[\alpha E + (1-\alpha)*C] \quad (25)$$

Where α is self-adjustable factor which can regulate the whole operation. E is the error of the system, C is the change in error and u is the control variable.

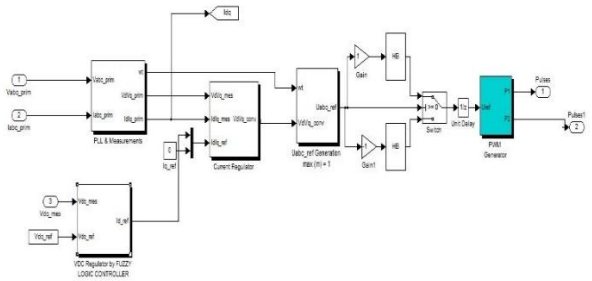

Fig. 10(a) Two level switching scheme control by using fuzzy logic controller.

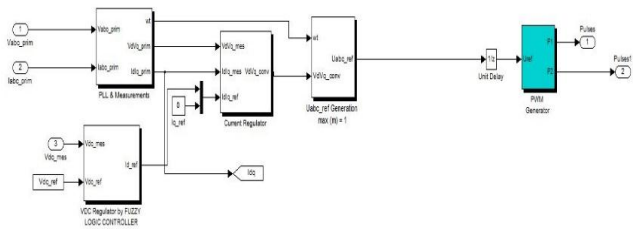

Fig. 10(b) Forced switching scheme control by using fuzzy logic controller.

In existing model, we use the PI controller technique to control the perturbations in the both the schemes. In this proposed sliding mode controller schemes, instead of using the PI controller we implemented the FUZZY LOGIC CONTROLLER technique and their related figures are shown in fig.10(a) and fig.10(b).

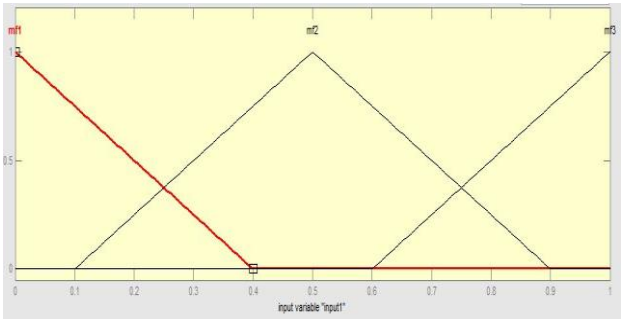

Fig 11.input error as membership functions

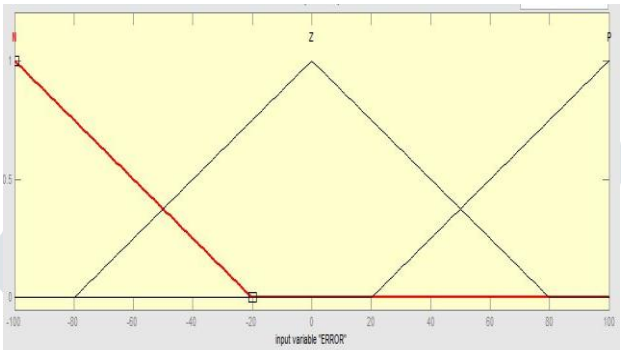

Fig.12 change as error membership functions

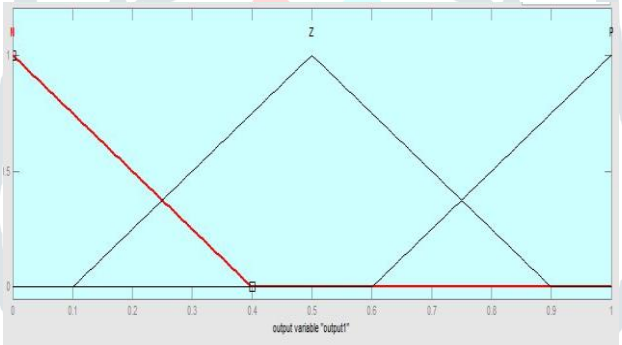

Fig.13 output variable Membership functions

V. RESULTS OF THE PROPOSED SMC SCHEME

The complete grid-connected photovoltaic (PV) system, based on the CTLI, has been simulated in the MATLAB / Simulink environment by using FLC. The active and reactive power deliveries in response to the variations of solar level are shown in the following subsections.

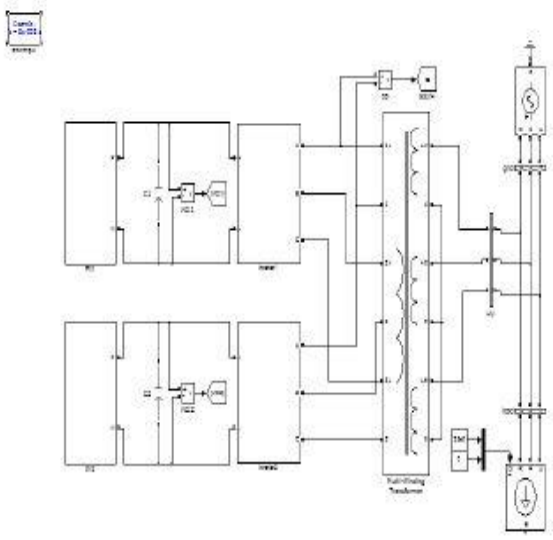

Fig.14.Block diagram of simulation

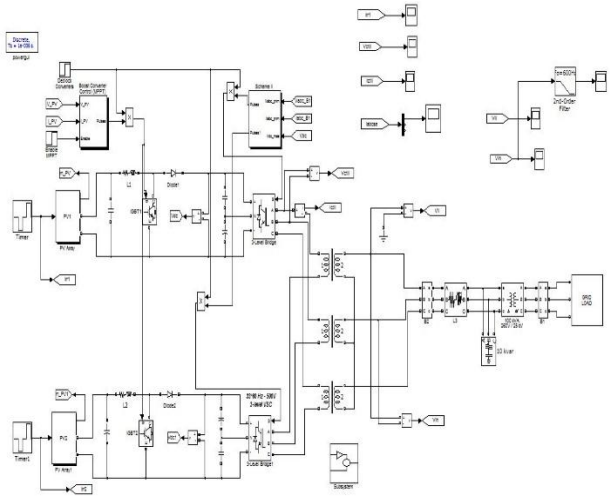

Fig.15 Control block diagram of simulation

A. Active power variation for two switching schemes

Fig. 16 (a) shows the output voltage of the voltage source CTLI when using the two-level switching scheme. Fig. 16 (b) shows the three-phase output currents of the CTLI. The current is analyzed for harmonic spectrum is given in Fig. 16 (c). The voltage (ea, eb, and ec) is applied across the low-voltage (LV) side of the transformer.

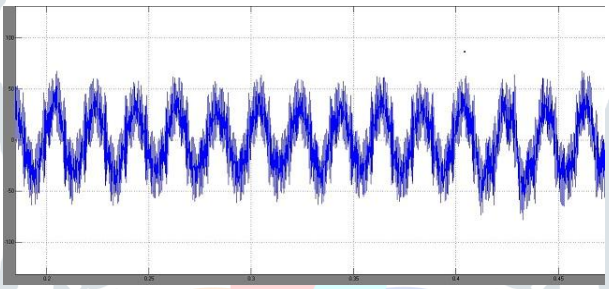

Fig 16 (a): CTLI Output Voltage for Scheme -I

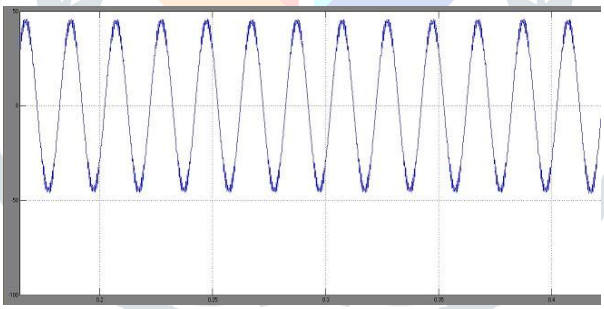

Fig 16 (b): CTLI Output Current for Scheme – I

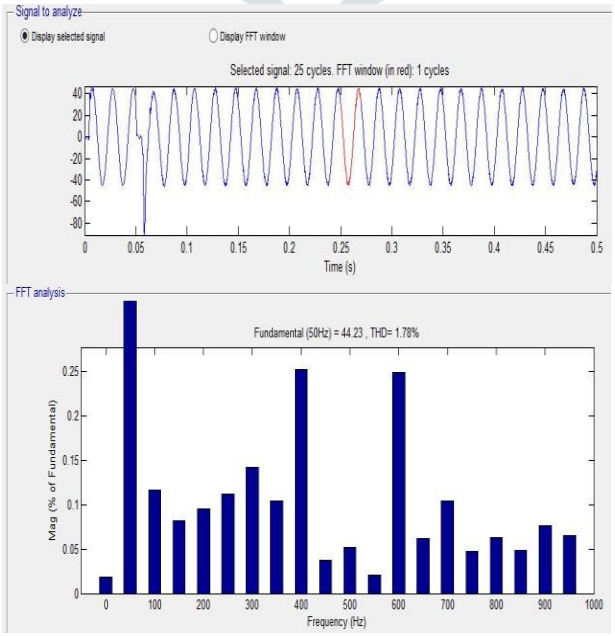

Fig 16 (c): Harmonic Spectrum of output Current

Scheme – I

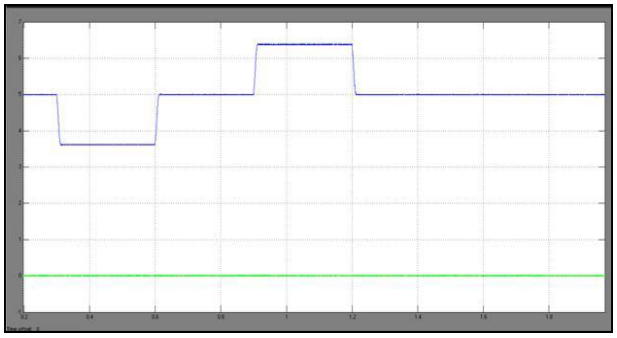

Fig 17 (a): direct axis and quadrature axis inverter current

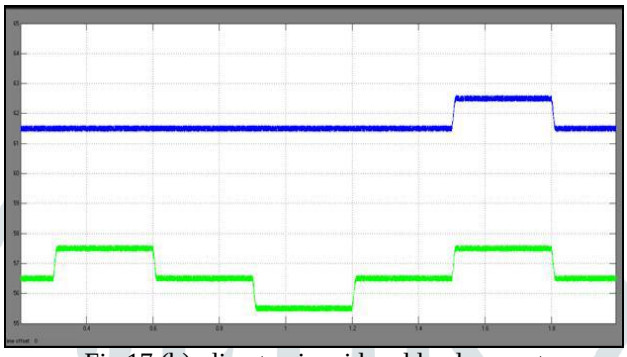

Fig 17 (b): direct axis grid and load current

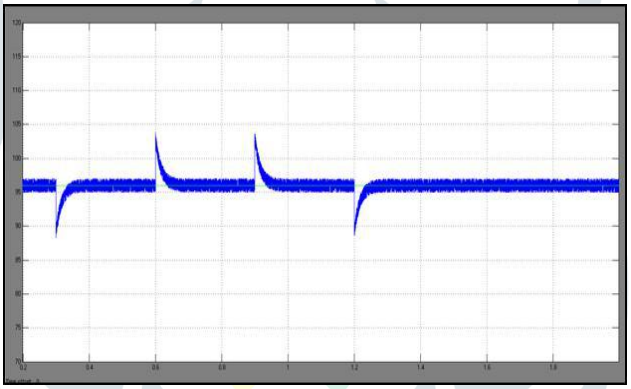

Fig 17 (c): dc-link voltage for scheme –I

B. Active power variation for forced switching schemes

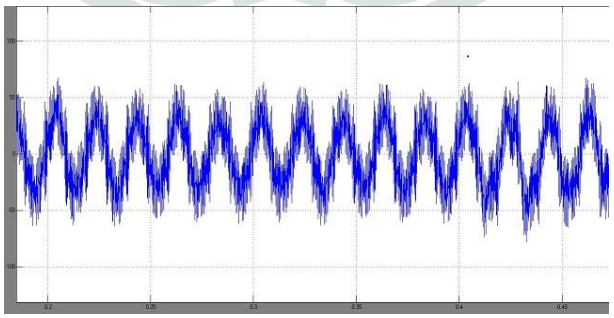

Fig 18 (a): CTLI Output Voltage for Scheme –II

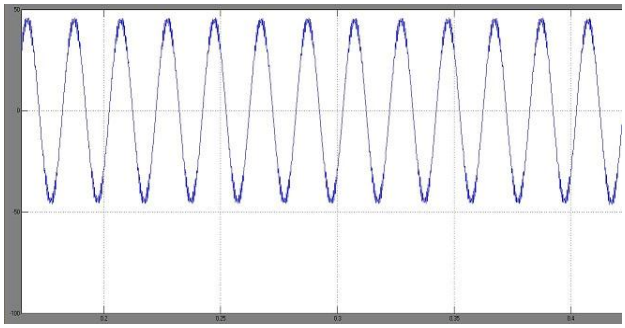

Fig 18 (b): CTLI Output Current for Scheme –II

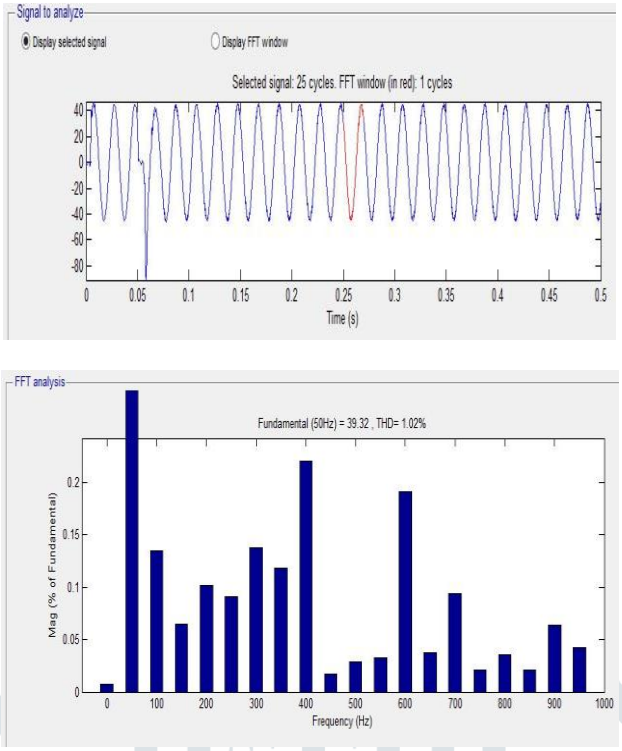

Fig 18 (c): Harmonic Spectrum of Output Current for Scheme-II

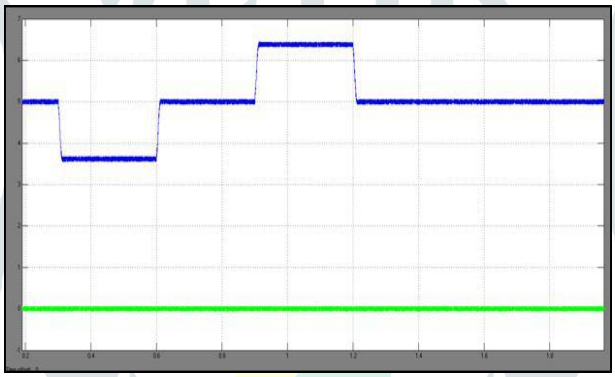

Fig 19 (a): direct axis and quadrature axis inverter current

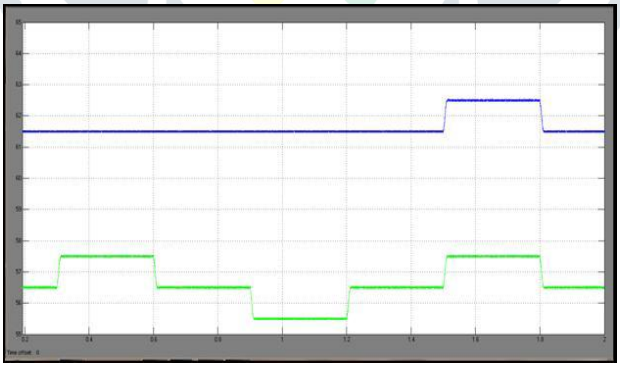

Fig 19 (b): direct axis grid and load current

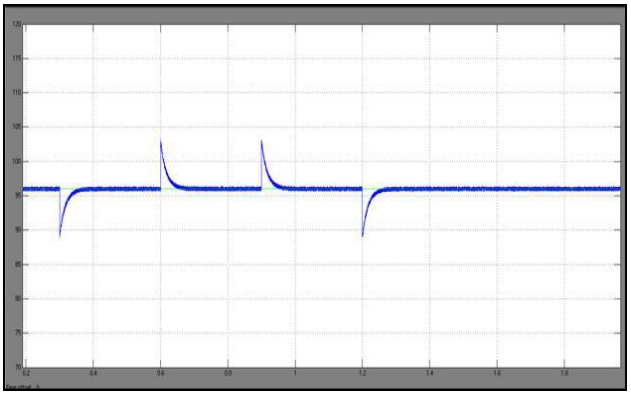

Fig 19 (c): dc-link voltage for forced switching scheme

The operation is found to supply varying active power and no reactive power, ensuring maximum utilization of the system.

C: SIMULATED INVERTER OUTPUTS

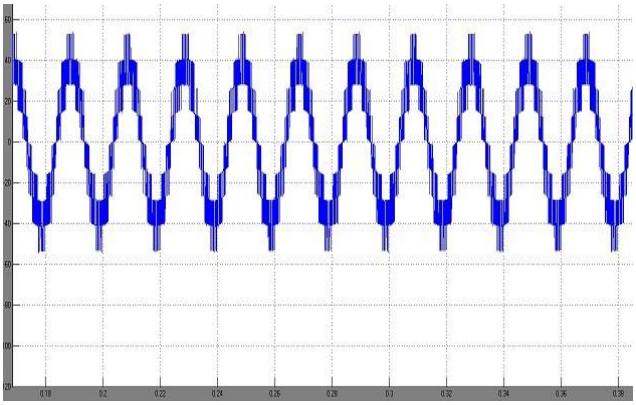

Fig 20 (a): Line to Line Voltage

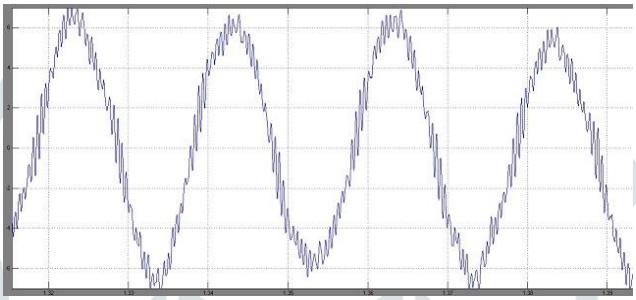

Fig 20 (b): Line Current

TABLE III

TYPE OF CONTROLLER	TOTAL HARMONIC DISTORTION FACTOR	
	SCHEME-I	SCHEME-II
PI CONTROLLER	4.79%	1.78%
FUZZY LOGIC CONTROL	1.78%	1.02%

VI. CONCLUSION

In this chapter, active and reactive power supply to the grid connected PV system and the THD were effectively improved by using the FLC technique were studied. The dynamic performance of the system is improved by introducing the inner current loop. Basically we use the inverter control loop for maintaining good voltage regulation and achieving fast dynamic response under sudden load fluctuations. Sliding Mode Controller can be used for current control of the PWM inverter in order to address the issues of utility grid connection. . Here the performance of the CTLI is found out to be satisfactory for two different control schemes of SMC. The controller is shown to extract maximum power from the solar PV modules by maintaining the dc-link voltage at the desired level for both the schemes. This ensures the utilization of the PV system for both active and reactive power delivery with the proposed SM controller. Thus, the active and reactive power supply to the grid are with in specified limits. In addition, the THD factor was improved effectively by using the FUZZY LOGIC CONTROLLER technique instead of PI controller were shown in TABLE III.

REFERENCES

[1] J.M. Carrasco, L.G. Franquelo, J.T. Bialasiewicz, E. Galván, R.C.P. Guisado, M.Á.M. Prats, J.I. León, and N.M. Alfonso, "Power-electronic systems for the grid integration of renewable energy sources: A survey," *IEEE Trans. Ind. Electron.* vol. 53, no. 4, pp. 1002-1016, Aug. 2006.

[2] B. Sahan, S.V. Araujo, C. Noding, and P. Zacharias, "Comparative Evaluation of Three-Phase Current Source Inverters for Grid Interfacing of Distributed and Renewable Energy Systems" *IEEE Trans. Power Electron.*, Vol. 26, no. 8, pp. 2304 - 2318, 06 Dec. 2010.

[3] S. Kouro, J.I.Leon, D.Vinnikov and L.G. Franquelo, "Grid-Connected Photovoltaic Systems an overview of Recent Research and Emerging PV Converter Technology," *IEEE Ind. Electron. Mag.*, vol. -9, no-1, pp.-47-61, 19 Mar.2015.

[4] F. Blaabjerg, Z. Chen, and S. B. Kjaer, "Power electronics as efficient interface in dispersed power generation systems," *IEEE Trans. Power Electron.*, vol. 19, no. 5, pp. 1184–1194, Sept.2004.

[5] V.F. Pires, J.F. Martins, and C. Hao, "Dual-inverter for grid-connected photovoltaic system: Modeling and sliding mode control," *Elsevier Solar Energy*, vol. 86, no.7, pp. 2106-2115, July 2012.

[6] A. Edpuganti, and A.K. Rathore, "New Optimal Pulse width Modulation for Single DC-Link Dual-Inverter Fed Open-End Stator Winding Induction Motor Drive," *IEEE Trans. Power Electronics*, Vol.30, no. 8, pp.4386 - 4393, Aug. 2015.

[7] N. Kumar, T.K. Saha, and J. Dey, "Cascaded Two Level Inverter Based Grid Connected Photovoltaic System: Modeling and Control," *IEEE International Conference on Industrial Technology (ICIT)*, Feb.26-Mar.1, 2014, Busan, Korea, pp. 468-473.

[8] G. Grandi, C. Rossi, D. Ostojic, and D. Casadei, "A New Multilevel Conversion Structure for Grid-Connected PV Applications", *IEEE Trans. Ind. Electron.*, vol. 56, no. 11, pp.4416-4426,Nov. 2009.

[9] V. Utkin, J. Guldner, and J. Shi, "*Sliding Mode Control in Electromechanical Systems*, "London, U.K: *Taylor and Francis*, 2009.

[10] K. K. Mohaptra, K. Gopakumar, and V. T. Somasekhar, and L. Umanand, "A harmonic elimination and suppression scheme for an open-end winding induction motor drive," *IEEE Trans. Ind. Electron..*, vol. 50, no. 6, pp. 1187-1198,Dec. 2003

[11] M.G. Villalva, J.R. Gazoli, and E.R. Filho, "Comprehensive Approach to Modeling and Simulation of Photovoltaic Arrays," *IEEE Trans. Power Electron.*, vol. 24, no. 5, pp.1198-1208, May 2009.

[12] J. A. Gow, and C.D. Manning, "Development of a photovoltaic array model for use in power-electronics simulation studies," *IEE Proc. Electr. Power Appl.*, vol. 146, no.2, pp.193-200, March 1999.

[13] S. A. Rahman1, R. K. Varma1 and T. Vanderheide, "Generalised model of a photovoltaic panel" *IET Renewable Power Generation*, Vol. 8, Iss. 3, pp.-217-229,August 2013.

[14] D. Cruz-Martins and R. Demonti. Photovoltaic energy processing for utility connected system. In *27th Annual Conference of the IEEE Industrial Electronics Society*, pages 1292–1296, 2011.

[15] H. B. Ertan, E. Dogru, and A. Yilmaz. Comparison of e ciency of two dc-to-ac converters for grid connected solar applications. In *OPTIM, 2012 13th International Conference on*, pages 879–886, 2012.

[16] J. H. R. Enslin and P. J. M. Heskes. Harmonic interaction between a large number of distributed power inverters and the distribution network. In *Proc. IEEE PESC'03*, pages 1742–1747, 2003.

[17] D. Meneses, F. Blaabjerg, O. Garcia, and J. A. Cobos. Review and comparison of step-up transformerless topologies for photovoltaic ac— module application. *IEEE Trans. Power Electron.*, 28(6):2649–2663, Jun. 2013.